THE JOURNAL OF BIOLOGICAL CHEMISTRY VOL. 287, NO. 50, pp. 42042–42052, December 7, 2012

Stromal Interaction Molecule 1 (STIM1) Is Involved in the Regulation of Mitochondrial Shape and Bioenergetics and Plays a Role in Oxidative Stress*

Received for publication, September 8, 2012 Published, JBC Papers in Press, October 17, 2012, DOI 10.1074/jbc.M112.417212

Nadine Henke[‡], Philipp Albrecht[‡], Annika Pfeiffer[‡], Diamandis Toutzaris[‡], Klaus Zanger[§], and Axel Methner[‡¶1]

From the [‡]Department of Neurology and the [§]Center for Anatomy and Brain Research, Medical Faculty, Heinrich Heine Universität Düsseldorf, D-40225 Düsseldorf, Germany and the [¶]Focus Program Translational Neuroscience, Rhine Main Neuroscience Network, Johannes Gutenberg University Medical Center Mainz, Department of Neurology, D-55131 Mainz, Germany

Background: Store-operated Ca^{2+} entry is regulated by the sensor STIM1 and the channel ORAI1.
Results: Deficiency alters mitochondrial shape and increases mitochondrial activity resulting in increased susceptibility to oxidative stress and cell death by nuclear translocation of apoptosis-inducing factor.
Conclusion: Store-operated Ca^{2+} entry regulates mitochondrial function and vulnerability.
Significance: STIM1 plays a role in oxidative stress by regulating mitochondrial function.

Calcium ions are involved in a plethora of cellular functions including cell death and mitochondrial energy metabolism. Store-operated Ca^{2+} entry over the plasma membrane is activated by depletion of intracellular Ca^{2+} stores and is mediated by the sensor STIM1 and the channel ORAI1. We compared cell death susceptibility to oxidative stress in STIM1 knock-out and ORAI1 knockdown mouse embryonic fibroblasts and in knock-out cells with reconstituted wild type and dominant active STIM1. We show that STIM1 and ORAI1 deficiency renders cells more susceptible to oxidative stress, which can be rescued by STIM1 and ORAI1 overexpression. STIM1 knock-out mitochondria are tubular, have a higher Ca^{2+} concentration, and are metabolically more active, resulting in constitutive oxidative stress causing increased nuclear translocation of the antioxidant transcription factor NRF2 triggered by increased phosphorylation of the translation initiation factor eIF2α and the protein kinase-like endoplasmic reticulum kinase PERK. This leads to increased transcription of antioxidant genes and a high basal glutathione in STIM1 knock-out cells, which is, however, more rapidly expended upon additional stress, resulting in increased release and nuclear translocation of apoptosis-inducing factor with subsequent cell death. Our data suggest that store-operated Ca^{2+} entry and STIM1 are involved in the regulation of mitochondrial shape and bioenergetics and play a role in oxidative stress.

Calcium ions are involved in a plethora of cellular functions ranging from short term responses such as contraction and secretion to long term regulation of cell growth and proliferation. Within the cell, Ca^{2+} is mainly stored in the endoplasmic reticulum (ER)[2] from where it is released upon activation of cell surface receptors and subsequent generation of the second messenger inositol 1,4,5-triphosphate, which binds and opens inositol 1,4,5-triphosphate receptors 1–3 at the ER membrane triggering Ca^{2+} release from the ER lumen. The following decrease in $[Ca^{2+}]_{ER}$ induces a strong Ca^{2+} influx from the extracellular space named store-operated Ca^{2+} entry (SOCE) (1, 2), which is followed by removal of cytosolic Ca^{2+} and replenishment of luminal Ca^{2+} through sarcoplasmic/endoplasmic reticulum Ca^{2+}-ATPases (SERCA). To ensure that the entering Ca^{2+} is promptly removed from the cytosol, subplasmalemmal mitochondria sequester parts of the entering Ca^{2+} ions and shuttle them to domains of the ER further apart from the membrane (3–5). As different enzymes of the Krebs cycle are activated by Ca^{2+} ions, mitochondrial Ca^{2+} uptake during activated SOCE increases matrix $[Ca^{2+}]$ and accelerates energy metabolism (6).

The Ca^{2+} sensor that conveys information about the Ca^{2+} load of the ER lumen to store-operated Ca^{2+} channels is stromal interaction molecule 1 (STIM1) (7, 8), a single transmembrane protein located in the ER membrane with a luminal EF hand and a cytosolic domain, which activates Ca^{2+} release-activated Ca^{2+} channels (7, 8). Upon store depletion, STIM1 clusters into punctae near the plasma membrane (9) and activates Ca^{2+} release-activated Ca^{2+} channels, mainly ORAI1 (10–12), resulting in a strong Ca^{2+} influx. Mutation of the luminal EF hand motif of STIM1 generates a constitutively active STIM1, which is located in punctae in close proximity to the plasma membrane and activates Ca^{2+} entry independently from ER Ca^{2+} stores (13, 14). In human embryonic kidney 293 cells, overexpression of ORAI1 alone inhibits SOCE, whereas expression of STIM1 alone just slightly increases Ca^{2+} entry during Ca^{2+} readdition after thapsigargin-induced store deple-

* This work was supported by Deutsche Forschungsgemeinschaft Grant ME1922/9-1 (to A. M.).
[1] To whom correspondence should be addressed: Johannes Gutenberg University Medical Center Mainz, Department of Neurology, Langenbeckstr. 1, D-55131 Mainz, Germany. Tel.: 49-6131-17-2695; Fax: 49-6131-17-5967; E-mail: axel.methner@gmail.com.
[2] The abbreviations used are: ER, endoplasmic reticulum; SOCE, store-operated Ca^{2+} entry; SERCA, sarcoplasmic/endoplasmic reticulum Ca^{2+}-ATPases; STIM1, stromal interaction molecule 1; MEF, mouse embryonic fibroblast; DA, dominant active; HBSS, Hanks' balanced salt solution; EYFP, enhanced yellow fluorescent protein; TMRE, tetramethylrhodamine ethyl ester; ANOVA, analysis of variance; BSO, L-buthionine-(*S*,*R*)-sulfoximine; ROS, reactive oxygen species; NRF, nuclear factor erythroid 2-related factor; KEAP, Kelch-like ECH-associated protein; PERK, protein kinase-like endoplasmic reticulum kinase; AIF, apoptosis-inducing factor.

tion. Only co-expression of ORAI1 and STIM1 increases SOCE pointing out the importance of the correct stoichiometry between STIM1 and ORAI1 (15). In addition to STIM1 and ORAI1, SERCA also co-assembles into punctae induced by store depletion and supposedly permits quick shuttling of entering Ca^{2+} into the ER (5, 16).

The link between Ca^{2+} and cell death is complex and has been extensively reviewed (17). Because STIM1 and ORAI1 are important players of SOCE, a link of these molecules to cell death appears possible and was investigated in different scenarios, yielding inconsistent results. STIM1 was first thought to be a tumor suppressor gene based on its genomic localization. In line with this hypothesis, transfection of STIM1 into cell lines derived from a rhabdoid tumor and a rhabdomyosarcoma-induced cell death (18). Similarly, inhibition of SOCE by siRNA-mediated knockdown of STIM1 increased survival of cervical epithelial cells on soft substrates (19). These reports suggested a negative effect of STIM1 and SOCE on cell survival. Malignant melanoma cells on the other hand were shown to depend on the intact SOCE machinery to sustain activation of the pro-survival factor protein kinase B/Akt (20) and silencing of STIM1-increased apoptosis of C6 glioma cells (21). Recently, Hawkins *et al.* (22) discovered that STIM1 can be glutathionylated in response to oxidative stress, which results in its constitutive activation and subsequent cell death.

In summary, the role of STIM1 in cell death still appears to be ambiguous. We therefore decided to compare cell death susceptibility to oxidative stress in STIM1 KO and WT mouse embryonic fibroblasts (MEFs) and in KO cells with reconstituted STIM1 and dominant-active STIM1 (DA-STIM1). Our data suggest that store-operated Ca^{2+} entry and STIM1 are involved in the regulation of mitochondrial shape and bioenergetics and play a role in oxidative stress.

EXPERIMENTAL PROCEDURES

Cell Culture—STIM1 KO and WT MEFs were a kind gift from Masatsugu Oh-Hora (Harvard University) and were cultured in DMEM high glucose with L-glutamine (PAA) containing 10% FCS (Thermo Fisher) and 100 units/ml penicillin and 100 μg/ml streptomycin (Invitrogen) and incubated in a humidified incubator with 5% CO_2 and 95% air. Stable cell lines were continuously selected using 1.5 mg/ml geneticin (Invitrogen).

Plasmids, siRNA, and Transfections—High purity plasmids pEYFP, STIM1-EYFP (8), STIM1-D76N/D78N-EYFP (14), and ORAI1-EYFP (a kind gift from Christoph Romanin, University of Linz, Linz, Austria) were prepared using Nucleobond AX 500 columns (Machery-Nagel). Flexitube siRNAs against ORAI1 were purchased from Qiagen (SI00972251 and SI00972258). Cells were grown to 70–80% confluency in 6-well plates and transfected with Attractene (Qiagen) in the case of plasmids or Lipofectamine RNAiMAX (Invitrogen) for siRNAs. Stable cell lines were generated by selection with geneticin and repeated fluorescence-activated cell sorting of EYFP positive cells on a MoFlo XDP (Beckman-Coulter).

Immunoblotting—The cells were lysed in ice-cold radioimmune precipitation assay buffer (Thermo Fisher Scientific) containing the mini complete protease inhibitor mixture (Roche Applied Science) and centrifuged for 30 min at 16,000 × *g*. The supernatants were separated on 8–16% polyacrylamide gels (Thermo Scientific), transferred onto nitrocellulose membranes using the iBlot System (Invitrogen), and blocked in 3% nonfat dry milk in phosphate-buffered saline or Tris-buffered saline for phosphorylation-sensitive antibodies containing 0.5% Tween 20 (PBS-T/TBS-T) for 1 h at room temperature. The membranes were incubated overnight with primary antibodies against STIM1 (Abnova, H00006786-M01, 1:1000), STIM2 (Cell Signaling, 4917, 1:1000), eIF2α (Cell Signaling, 9722, 1:1000), phospho-eIF2α (Cell Signaling, 9721, 1:1000), phospho-PERK (Cell Signaling, 3179, 1:1000), GAPDH (Cell Signaling, 2118, 1:5000), or actin (Millipore, MAB1501, 1:5000) followed by anti-mouse (rabbit) IgG (Fc) infrared fluorescence-conjugated (Licor, 1:30,000) secondary antibody. The membranes were scanned for infrared fluorescence at 680 or 800 nm using the Odyssey system (Licor). Intensity was quantitated with the image-processing software ImageJ.

Ca^{2+} Imaging—The cells were seeded in 24-well plates at a density of 100,000 cells per well and loaded 24 h later with Fura2-AM (Invitrogen) in HBSS (Invitrogen) at a concentration of 2 μM for 30 min at 37 °C. The cells were measured in HBSS or EGTA buffer (Ca^{2+}-free HBSS supplemented with 0.5 mM EGTA, 20 mM HEPES, 1 mM $MgCl_2$, and 1 g/liter glucose). Imaging was performed on an Olympus IX81 fluorescence microscope with cell^R imaging software. Images were taken at 340- and 380-nm excitation, and the ratio was calculated every 5 s for a period of 5 min for every single cell. The indicated substances were added 1 min after onset of the measurement.

For SOCE experiments, the cells were seeded on coverslips, loaded with Fura2, and placed into a flow chamber. Measurements were performed as described above. Base-line Ca^{2+} was recorded in HBSS for 2 min and then replaced by EGTA buffer with 2 μM thapsigargin to deplete ER Ca^{2+} stores. After 8 min, Ca^{2+} was readded by changing the buffer to HBSS again. In experiments with transfected cells, only EYFP-positive cells were analyzed.

Cell Survival Assays—The cells were seeded in 96-well plates at a density of 5000 cells/well in quintuplicate. Transiently transfected cells were seeded 24 h after transfection. Pharmacological agents were added the day after plating, and cell survival was quantified again 24 h later using the cell titer blue reagent (Promega). Either absorbance at 562 nm together with a reference value at 612 nm or fluorescence emission at 590 nm after exciting at 562 nm was measured using a GENios Pro microplate reader (Tecan). Alternatively, the cells were stained in DMEM without phenol red (PAA) with Hoechst 33342 (0.5 μg/ml; Sigma Aldrich) as a marker for all cells and Sytox Orange (0.5 μM; Molecular Probes) as a marker for dead cells and analyzed in a BD Pathway 855 high content imaging system (BD Bioscience). Regions of interest around the nuclei were defined by Hoechst signal, and double-positive cells were counted as dead cells.

GSH Assay—Total cellular GSH content was measured enzymatically recording NADPH consumption by GSH reductase. The cells, seeded in 6-well plates in duplicates on the day before the assay, were detached in 200 μl of PBS with EDTA, transferred into 100 μl of 10% sulfosalicylic acid, vortexed vigor-

ously, and incubated on ice for 10 min. After centrifugation for 10 min at 16,000 × *g*, the supernatants were transferred into 24 μl of 50% triethanolamine. The samples were diluted in an assay buffer containing 100 mM Na_2PO_4, 1 mM EDTA, pH 7.5, 0.6 mM 5,5′-dithiobis-(2-nitro-benzoic acid) and 0.8 mM NADPH. After addition of 1 unit/ml glutathione reductase, NADPH content was monitored at 390 nm using GENios Pro microplate reader (Tecan). Total cellular GSH was normalized to cellular protein amounts obtained from pellets after centrifugation solubilized in 100 μl of 0.2 N NaOH at 37 °C overnight analyzed with a BC assay protein quantification kit (Interchim).

Quantitative Real Time PCR—For expression analysis of antioxidant response genes, whole RNA was isolated using the ZR RNA MiniPrep Kit (Zymo) and subjected to cDNA synthesis with a high capacity cDNA reverse transcription kit (ABI). Real time analysis was performed on a 7500 Fast cycler (ABI) with FAST BLUE qPCR MasterMix (Eurogentec) running the 7500 standard program for TaqMan assays. Primers and probes for antioxidant response genes were designed by the universal probe library assay design center (Roche Applied Science). The hypoxanthine-phosphoribosyltransferase gene (*hprt*) served as endogenous control. Primers and *hprt* probe were purchased from MWG.

Mitochondrial Membrane Potential, Ca^{2+} Content, and Superoxide Production—Mitochondrial membrane potential, matrix Ca^{2+} content, and superoxide production were determined by flow cytometry using tetramethylrhodamine ethyl ester (TMRE) (Sigma), Rhod2-AM (ABD Bioquest), or dihydrorhodamine 6G (Invitrogen). The cells were seeded in 6-well plates in triplicate the day before the experiment. Staining was carried out at 37 °C in HBSS with 10 μM TMRE or 2 μM Rhod2-AM for 30 min or 1 μM dihydrorhodamine 6G for 15 min. After two wash steps, mean red fluorescence was analyzed on a FACSCalibur flow cytometer (BD Biosciences).

Immunofluorescence Staining and Nuclear Translocation Assay—The cells were seeded in 96-well imaging plates (BD Biosciences) coated with 0.1% gelatin and for AIF translocation assays subjected to glutamate treatment overnight 24 h later. For NRF2 staining, the cells were left untreated. After fixation in 4% paraformaldehyde for 10 min at 37 °C, the cells were permeabilized in 1× blocking solution (Roti-Block diluted in PBS; Carl Roth) supplemented with 0.1% Triton X-100 and subsequently incubated overnight in primary antibody solution (goat anti-AIF (D-20) sc-9416 from Santa Cruz or rabbit anti-NRF2 (H-300) sc-13032 from Santa Cruz both diluted 1:100 in blocking solution). After incubation with Cy3-labeled secondary antibody (Millipore) and nuclear staining with Hoechst 33342, nuclear translocation of AIF or NRF2 was measured on a BD Pathway 855 high content imaging system (BD Bioscience). Nuclear regions of interest were identified by Hoechst signal, and a concentric region around the nuclear region of interest was assessed as cytoplasm. The ratio of the nuclear and cytoplasmic Cy3 signal was calculated as the measure of translocation.

TEM Imaging—After trypsinization, the cells were pelleted, first fixed in 2.5% glutaraldehyde, 2% paraformaldehyde, and 0.05% tannic acid and afterward treated with 2% osmium tetroxide. After staining with 1.5% uranylacetate and 1.5% phosphotungstic acid, the pellets were embedded in epoxide resin (Spurr) and dissected in 70–80-nm-thick slices on an ultramicrotome (Reichert Ultracut, Vienna, Austria). Images (30 KO and 32 WT) were taken on a Hitachi H 600 transmission electron microscope in 15,000× magnification. Distances between mitochondria and ER membranes, as well as the length of the mitochondrial cut surface, were measured with the image analysis software Axiovision (Zeiss). In total, 523 mitochondria were analyzed for each cell type.

Analysis of Mitochondrial Shape—To visualize mitochondria of STIM1 WT and KO fibroblasts, the cells were transfected with mitochondrially targeted dsRed2 (kind gift of Axel Niemann, Zürich, Switzerland) and transferred to coverslips 24 h post-transfection. Again, 24 h later, 2.5 mM of glutamate or vehicle was added to the cell culture medium. After 16 h cells were fixed in 4% paraformaldehyde, stained with Hoechst 33342, and mounted in fluorescence mounting medium (Dako). Analysis of mitochondrial morphology was performed on an Olympus IX81 fluorescence microscope with a 60× oil immersion objective. For each condition, 100 cells were counted and categorized dependent on their mitochondrial morphology.

Statistical Analysis—The data were summarized as the means ± S.E., and the statistical significance was calculated using two-tailed *t* tests or analysis of variance (ANOVA) with Tukey's multiple comparison post hoc test as indicated using Graphpad Prism software. p values <0.05 were considered significant.

RESULTS

SOCE Deficiency Renders Cells More Susceptible to Oxidative Stress—To evaluate our model for SOCE deficiency, we first confirmed that mouse embryonic fibroblasts derived from STIM1 KO mice indeed did not express STIM1 (Fig. 1*A*). These cells showed no compensatory up-regulation of the STIM1 homologue STIM2 (Fig. 1*B*) and exhibited a remarkable reduction of Ca^{2+} re-entry after store depletion with the SERCA inhibitor thapsigargin compared with wild type control cells generated and passaged in parallel (Fig. 1*C*). We concluded that these cells constitute an adequate model of chronic SOCE deficiency and studied their susceptibility to oxidative stress using the model of oxidative glutamate toxicity, which is an excellent model of endogenous oxidative stress (23). In this paradigm, large amounts of extracellular glutamate block the glutamate-cystine antiporter system Xc^-. This leads to deprivation of cystine and its reduced form cysteine, the rate-limiting substrate for the synthesis of GSH, the most important intracellular antioxidant. The subsequent GSH depletion leads to accumulation of reactive oxygen species and cell death by oxidative stress (recently reviewed in Ref. 23). We also blocked GSH synthesis directly by using the glutamate-cysteine ligase inhibitor BSO (L-buthionine-(*S*,*R*)-sulfoximine). In all assays, cell viability was quantitated by survival assays utilizing reduction of resazurin to resorufin through metabolic activity of healthy cells. Using these paradigms, we observed an increased sensitivity of STIM1 KO MEFs to oxidative stress compared with WT MEFs (Fig. 1*D*). To rule out artifacts brought about by the resazurin method, we confirmed the results with an inde-

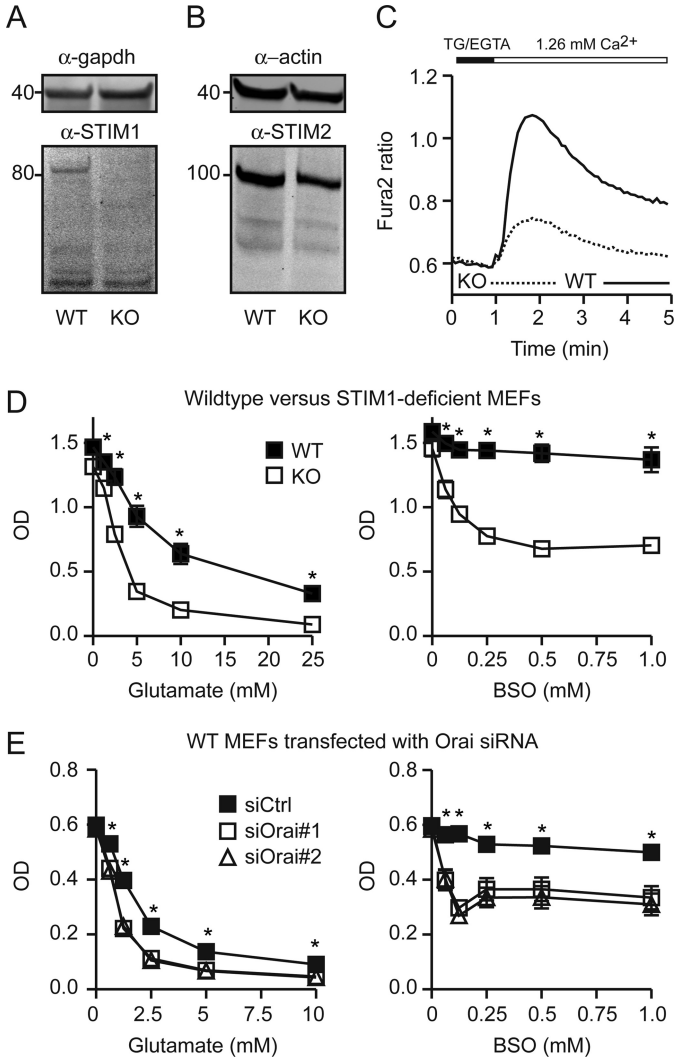

FIGURE 1. **SOCE deficiency renders cells more susceptible to oxidative stress.** *A* and *B*, immunoblots of STIM1 WT and KO cell lysates show lack of STIM1 (*A*) and no compensatory up-regulation of STIM2 (*B*). GAPDH and actin served as loading controls. Size is indicated. *C*, reduction of SOCE in STIM1 KO cells was quantitated by single cell microscopy using fura2-AM. Graphs show mean fura2 ratio of 164 (WT) and 170 (KO) cells. ER Ca^{2+} stores were emptied with 2 μM thapsigargin in Ca^{2+}-free conditions before readdition of HBSS containing 1.26 mM Ca^{2+}. Traces show only Ca^{2+} readdition. *D*, viability of STIM1 WT and KO cells treated for 16 h with the indicated concentrations of oxidative stress inductors glutamate or BSO. *E*, survival of WT cells transfected 48 h before oxidative stress induction with two independent siRNAs against ORAI1 or control siRNA. *D* and *E*, viability was quantitated by the cell titer blue assay. The graphs show mean ± S.E. absorbance values of 15 replicates for each condition obtained in three independent experiments. *, $p < 0.05$, Student's *t* test (*D*) or ANOVA with Tukey's post hoc test (*E*).

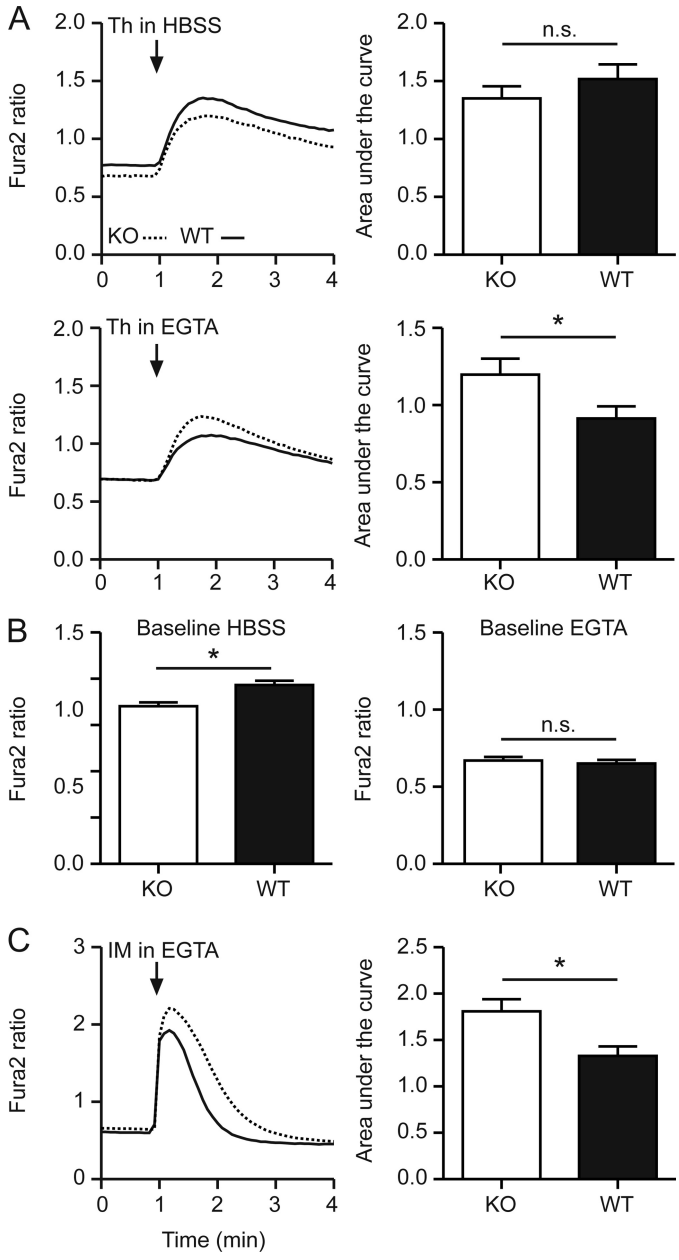

FIGURE 2. **Effects of STIM1 deficiency on the intracellular Ca^{2+} homeostasis.** fura2 single-cell imaging of WT and STIM1 KO cells. After 1 min of base-line recording, 2 μM thapsigargin (*A*) or 5 μM ionomycin (*C*) was added as indicated, and the fura2 signal was recorded for an additional 4 min. The graphs show mean fura2 ratio of >150 cells for each condition. For all experiments, the area under the curve (*A* and *C*) and the base-line fura2 ratio (*B*) of the first minute of measurement was calculated and plotted as the means ± S.E. *n.s.*, not significant; *, $p < 0.05$, Student's *t* test.

pendent method using high content imaging of live and dead cells stained with the dead cell marker Sytox Orange and Hoechst 33342 as a marker for all cells (not shown). We also reproduced these results by knocking down the other essential component of SOCE, ORAI1, the pore-forming subunit of store-operated Ca^{2+} channels. Consistent with the results obtained in the STIM1 knock-out condition, siRNA-mediated knockdown of ORAI1 in WT MEFs resulted in an increased susceptibility to oxidative stress induced by glutamate or BSO (Fig. 1*E*).

For a complete characterization of these cells, we also examined the thapsigargin-releasable Ca^{2+} pool in the presence and absence of extracellular Ca^{2+} as a measure of the ER $[Ca^{2+}]$ and the total cellular Ca^{2+} content by treatment with the Ca^{2+} ionophore ionomycin (Fig. 2). These experiments showed that STIM1 deficiency decreases slightly the cytosolic base-line Ca^{2+} and increases the total cellular Ca^{2+} content. We concluded that the intact SOCE machinery is important for cell survival under oxidative stress conditions and tried to rescue the phenotype by overexpressing wild type or dominant active STIM1 in STIM1 KO cells.

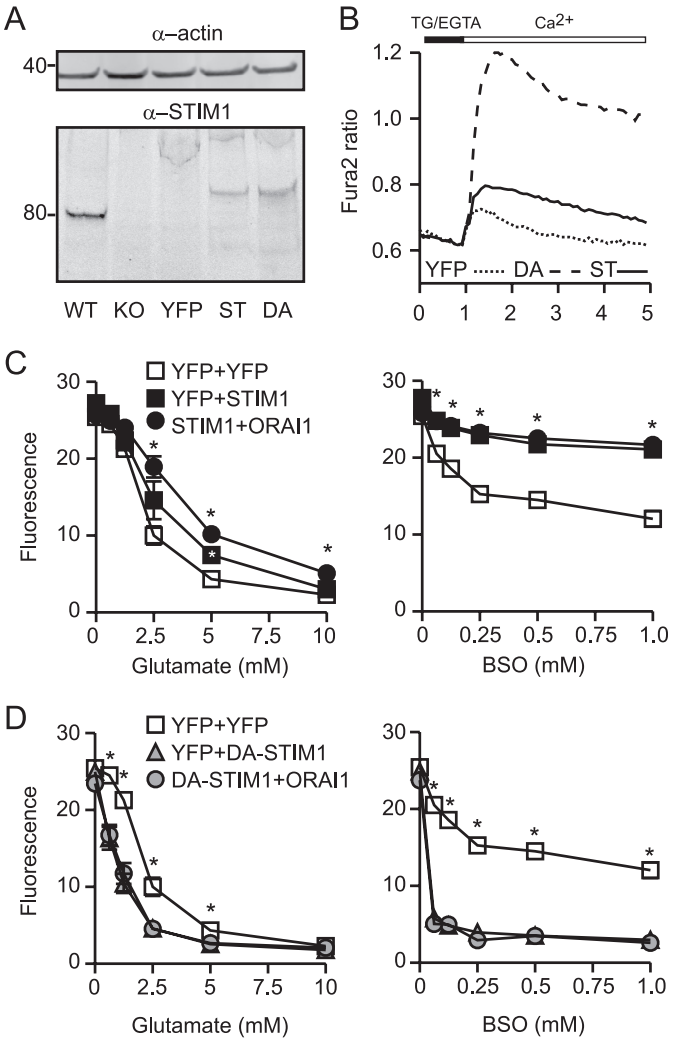

FIGURE 3. **STIM1 expression in STIM1 KO cells restores SOCE and protects from oxidative stress.** *A*, STIM1 KO MEFs were stably transfected with STIM1-EYFP (*ST*), dominant active DA-STIM1-EYFP (*DA*), or YFP, and the expression was verified by immunoblotting. Actin served as loading control. Size is indicated. *B*, reconstitution of SOCE quantitated by single cell microscopy using fura2-AM after ER Ca^{2+} stores were emptied with 2 μM thapsigargin in Ca^{2+}-free conditions. Graphs show mean fura2 ratio of 78 (*YFP*), 70 (STIM1-EYFP, *ST*), or 63 (DA-STIM1-EYFP, *DA*) cells. Traces show only Ca^{2+} readdition. *C* and *D*, survival of stably STIM1-EYFP (*C*) or DA-STIM1-EYFP (*D*) expressing STIM1 KO MEFs, additionally transfected with ORAI1-EYFP or YFP 48 h before induction of oxidative stress by glutamate or BSO. Viability in *C* and *D* was quantitated by the cell titer blue assay 16 h after addition of the indicated drugs. The graphs show the means ± S.E. of 15 replicates for each condition obtained in three independent experiments. *, $p < 0.05$, ANOVA with Tukey's post hoc test.

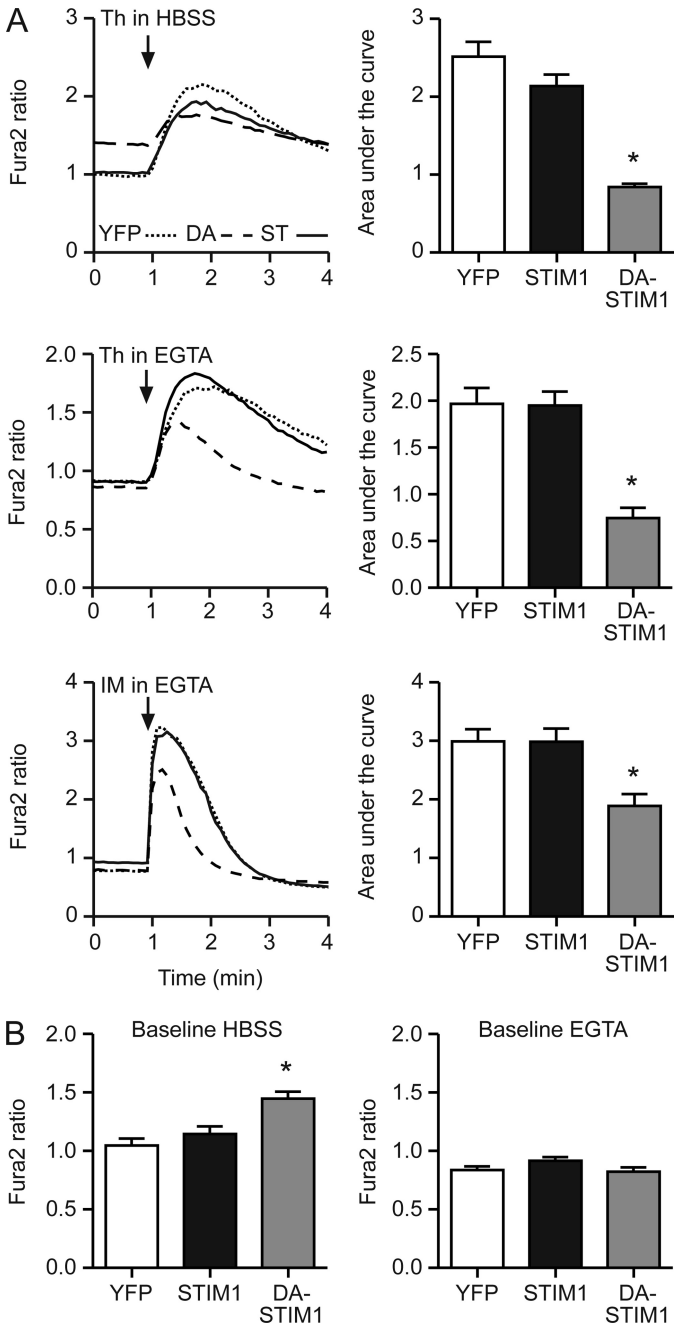

FIGURE 4. **Effects of STIM1 rescue on the intracellular Ca^{2+} homeostasis.** *A*, Fura2 single cell imaging of stably STIM1-EYFP or DA-STIM1-EYFP expressing STIM1 KO MEFs. After 1 min of base-line recording, 2 μM thapsigargin or 5 μM ionomycin was added as indicated, and the fura2 signal was recorded for additional 4 min. The graphs show mean fura2 ratio of >150 cells for each condition. For all experiments, the area under the curve (*A*) and the base-line fura2 ratio (*B*) of the first minute of measurement were calculated and plotted as the means ± S.E. *n.s.*, not significant; *, $p < 0.05$, ANOVA with Tukey's post hoc test.

STIM1 Expression in STIM1 KO Cells Restores SOCE and Protects from Oxidative Stress—We stably transfected STIM1-EYFP, DA STIM1-D76N/D78N-EYFP (14), or EYFP alone into STIM1 KO MEFs and verified the expression by immunoblotting (Fig. 3*A*). In line with the presumed dominant active phenotype of DA-STIM1, we observed an increased SOCE in DA-STIM1-EYFP > STIM1-EYFP > EYFP (Fig. 3*B*). This demonstrated a successful overexpression of both STIM1 isoforms. Survival assays with transfected cells showed that STIM1-EYFP-overexpressing cells were protected against oxidative glutamate toxicity and GSH depletion induced by BSO (Fig. 3*C*), which was even further increased by transient co-transfection of ORAI1-EYFP in the case of oxidative glutamate toxicity (Fig. 3*C*). DA-STIM1-EYFP-transfected cells, in contrast, were more susceptible to both stressors, which was independent of ORAI1 because transient ORAI1-EYFP co-expression had no further effect on the resistance of these cells (Fig. 3*D*).

We also examined the thapsigargin-releasable Ca^{2+} pool and the total cellular Ca^{2+} content in these cells and observed no differences between EYFP and STIM1-EYFP (Fig. 4*A*).

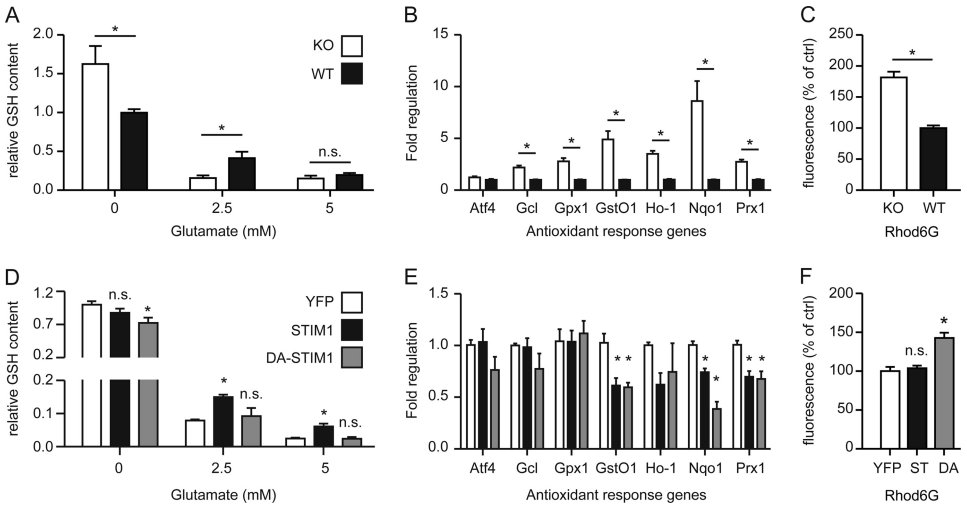

FIGURE 5. **Increased oxidative stress in STIM1 KO cells is overcompensated under basal conditions.** *A* and *D*, enzymatic determination of whole cellular GSH content in STIM1 WT and KO MEFs (*A*) or stably STIM1-EYFP and DA-STIM1-EYFP transfected KO cells (*D*) treated with the indicated concentrations of glutamate for 8 h in three independent experiments. GSH concentrations were normalized to cellular protein content and plotted as GSH content relative to untreated WT or YFP sample as the means ± S.E. *B* and *E*, real time RT-PCR analysis of mRNA levels of indicated antioxidant response genes in STIM1 WT and KO cells (*B*) or stably STIM1-EYFP expressing KO MEFs (*E*). The signals were normalized to *hprt* mRNA abundance and plotted in bar graphs as fold regulation over WT and EV samples. *C* and *F*, cellular ROS load of WT and STIM1 KO MEFs (*C*) or stably empty vector (*YFP*), STIM1-EYFP (*ST*), or DA-STIM1-EYFP (*DA*) expressing STIM1 KO MEFs (*F*) was quantitated by flow cytometry using rhodamine-6G fluorescence. The *bar graphs* represent mean relative fluorescence over WT and EYFP ± S.E. of three independent experiments each performed in triplicate. *n.s.*, not significant; *, $p < 0.05$, Student's *t* test (*A–C*) or ANOVA with Tukey's post hoc test (*D–F*).

DA-STIM1-EYFP, however, induced a reduction in ER and total cellular Ca^{2+} and a substantial increase of the base-line cytosolic [Ca^{2+}] in the presence of extracellular Ca^{2+} (Fig. 4*B*).

Our data suggest that STIM1 and SOCE play a role in oxidative stress, which is probably not mediated via the changes in the thapsigargin-releasable Ca^{2+} pool and the total cellular Ca^{2+} content. Also, STIM1 activation can apparently become detrimental, as shown by the deleterious effects of DA-STIM1-EYFP, which implies that SOCE must be delicately balanced and regulated to avoid unfavorable overactivation.

Increased Oxidative Stress in STIM1 KO Cells Is Overcompensated under Basal Conditions—In oxidative glutamate toxicity, cell death is mediated by GSH depletion. We therefore quantitated the GSH content of WT and STIM1 KO MEFs before and after glutamate challenge, which showed an elevated base-line GSH in STIM1 KO cells that nevertheless dropped to significantly lower levels after glutamate treatment (Fig. 5*A*). This increased GSH content at base line was also reflected by increased basal transcription of genes involved in the antioxidant response quantitated by real time PCR (Fig. 5*B*). We observed a significant up-regulation of glutamate-cysteine ligase (*Gcl*), glutathione peroxidase 1 (*Gpx1*), glutathione *S*-transferase ω-1 (*GstO1*), heme-oxygenase 1 (*Ho-1*), NAD(P)H quinone oxidoreductase 1 (*Nqo1*), and peroxiredoxin 1 (*Prx1*). These data suggested that STIM1 deficiency causes constitutive oxidative stress, which is counteracted by an up-regulation of the antioxidant response battery, which can still not cope with additional exogenous oxidative stress. We therefore quantitated reactive oxygen species (ROS) produced by the mitochondria of STIM1 KO and WT cells by using the fluorescent dye dihydrorhodamin 6G. In line with our hypothesis, we observed an increased ROS content of STIM1 KO mitochondria (Fig. 5*C*).

We were able to rescue these effects in our stably transfected cells. Here, DA-STIM1-EYFP overexpression had a negative effect on base-line GSH, whereas only STIM1-EYFP overexpression but not DA-STIM1-EYFP preserved GSH content after glutamate challenge (Fig. 5*D*). The induction of the antioxidant response gene expression was also significantly reversed for *GstO1*, *Nqo1*, and *Prx1* but not for *Gcl*, *Gpx1*, and *Ho-1* without a significant difference between the two STIM1 variants suggesting additional factors (Fig. 5*E*). The base-line mitochondrial ROS production, in contrast, was again similar to base-line GSH content, not different between EYFP and STIM1-EYFP-expressing cells but significantly increased in cells expressing the detrimental dominant active variant of STIM1 (Fig. 5*F*). We conclude that lack of STIM1, as well as constitutive STIM1 activity, results in an imbalance of ROS production and detoxification.

The Up-regulated Antioxidant Response in STIM1 KO Cells Is Mediated via NRF2 and Phosphorylated eIF2α—To identify the mechanisms responsible for the observed up-regulation of the antioxidant response battery in STIM1 KO cells, we considered enhanced expression and translocation of the transcription factor nuclear factor erythroid 2-related factor 2 (NRF2), which binds to antioxidant response elements in the promoters of the up-regulated protective genes. By high content fluorescence microscopy, we quantitated NRF2 immunofluorescence intensity in the nucleus, which was identified by Hoechst staining, and the surrounding cytoplasm resembled by a concentric ring around the nucleus (Fig. 6*A*). The ratio of nuclear fluorescence to cytoplasmic fluorescence serves as a quantitative and very sensitive measure for nuclear translocation. NRF2 was indeed found to be significantly increased in the nucleus of STIM1 KO cells (Fig. 6*A*). NRF2 is known to be regulated by Kelch-like ECH-associated protein 1 (KEAP1), which under normal con-

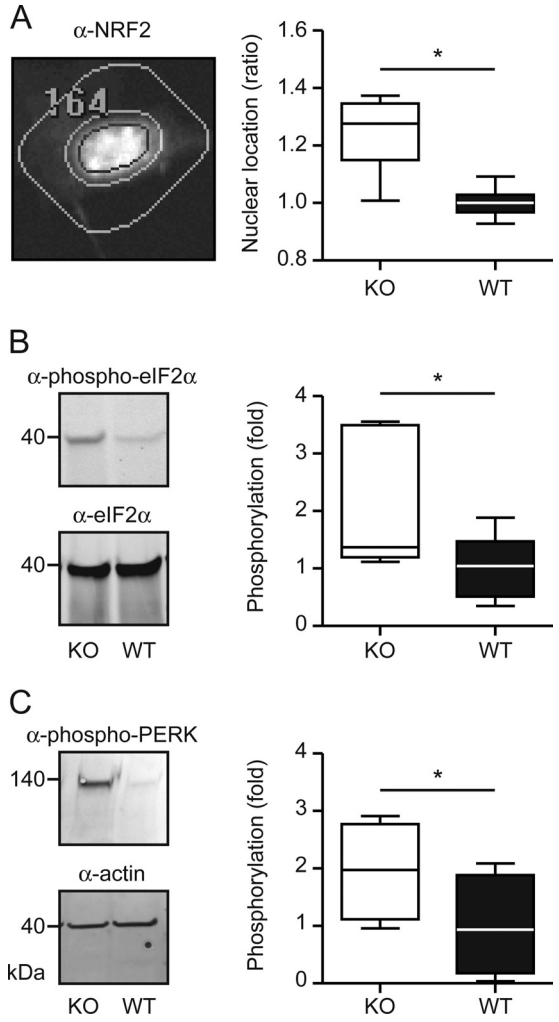

FIGURE 6. **The up-regulated antioxidant response in STIM1 KO cells is mediated via NRF2 and phosphorylated eIF2α.** *A*, translocation of NRF2 from the cytosol to the nucleus was analyzed by immunofluorescence in STIM1 WT and KO MEFs. NRF2 immunofluorescence intensity was quantified on a BD Pathway high content imaging system in the nucleus, which was identified by Hoechst staining, and the surrounding cytoplasm represented by a concentric ring around the nucleus. This method of segmentation is illustrated in the *left panel*. The ratio of nuclear to cytosolic NRF2 signal was calculated and normalized to WT signal. The graphs represent the means ± S.E. of 4468 WT and 3331 KO cells measured in three independent experiments each done in quintuplicates. *B* and *C*, immunoblot analysis of the phosphorylation state of eIF2α (*B*) or PERK (*C*). The blots were incubated with phosphorylation sensitive and insensitive antibodies against eIF2α (*B*) or phosphorylation-sensitive antibody against PERK and an antibody against actin as a loading control (*C*). Intensity values were calculated with the image analysis software ImageJ and normalized to WT control. The graphs represent the means ± S.E. of three independent experiments. *n.s.*, not significant; *, $p < 0.05$, Student's *t* test.

ditions binds NRF2 in the cytoplasm and marks it for degradation by the proteasome system (24). An increase in the cellular ROS level is sensed by KEAP1 through reactive cysteine groups, resulting in release of NRF2, which then translocates to the nucleus and activates antioxidant genes (25). Additionally, NRF2 can be activated by phosphorylated PERK (26). We therefore examined the phosphorylation state of PERK and an established PERK substrate, eIF2α, which plays a role in protection against oxidative stress (27), by immunoblotting. Both proteins were significantly hyperphosphorylated in STIM1 KO MEFs compared with WT MEFs (Fig. 6, *B* and *C*), proposing that phosphorylated PERK triggers NRF2 translocation, resulting in increased expression of antioxidant response genes in STIM1 KO cells. Moreover, the phosphorylated form of eIF2a can activate system Xc^- expression via nuclear factor ATF4, contributing to oxidative stress defense (27).

We conclude from these data that STIM1 KO cells exhibit a strong basal activation of antioxidative defense mechanisms triggered by NRF2 translocation and system Xc^- up-regulation through eIF2α phosphorylation. Despite these defense mechanisms, STIM1 KO cells are not able to cope with additional oxidative stress challenges.

Mitochondria of STIM1 KO Cells Are More Densely Packed and Have a Tubular Shape—Mitochondria are the main source of ROS in living cells, and their shape and function is critically dependent on intracellular Ca^{2+} signaling. Mitochondria also influence SOCE signals by shuttling Ca^{2+} released from the ER back to this intracellular store, which prevents luminal depletion (28), and they have a role in relaying Ca^{2+} signals from the plasma membrane to the ER (3). We therefore investigated mitochondrial shape and relationship with other organelles in WT and STIM1 KO MEFs by transmission electron microscopy and recognized distinct morphological differences. KO mitochondria appeared smaller, thinner, and more densely packed (Fig. 7*A*). This difference was statistically significant because the diameter of KO mitochondria, which were sectioned in a random fashion, amounted to KO 432 ($n = 523$, S.E. ±7.651) and WT 547.7 nm ($n = 523$, S.E. ±8.258) (Fig. 7*B*). Possible hot spots of ER mitochondria cross-talk like the distance between the ER and mitochondria (Fig. 7*D*) or areas of direct contact defined by a distance of less than 100 nm (Fig. 7*C*) were identical between KO and WT cells.

Mitochondria constantly fuse and divide, resulting in distinct shapes ranging from tubular to fragmented. These processes are highly dynamic and important for mitochondrial bioenergetics and cellular survival (reviewed in Ref. 29). Glutamate toxicity was previously shown to cause mitochondrial fragmentation and perinuclear accumulation (30). We therefore investigated the mitochondrial shape in STIM1 KO and WT cells and changes in response to glutamate in more detail. We transfected KO and WT cells with a mitochondrial targeted red fluorescent protein and treated the cells with 2.5 mM glutamate or vehicle overnight. After fixation, the mitochondrial shape was analyzed by fluorescence microscopy, and 100 cells for each condition were categorized by a blinded investigator. Categories were defined as healthy cells with fragmented mitochondria, healthy cells with tubular mitochondria, apoptotic cells with fragmented mitochondria, or apoptotic cells with tubular mitochondria (Fig. 7*E*). This analysis revealed a more tubular shape for mitochondria of STIM1 KO cells under basal conditions and also after overnight exposure to glutamate (Fig. 7*F*). Apparently, STIM1 KO cells possess more densely packed and elongated mitochondria, which raised the question about their metabolic activity.

Mitochondria from STIM1 KO Cells Are More Metabolically Active and More Susceptible to Nuclear Translocation of Apoptosis-inducing Factor—We therefore studied mitochondrial function by staining WT and KO cells with the mitochondrial Ca^{2+} reporter Rhod2-AM or the mitochondrial membrane

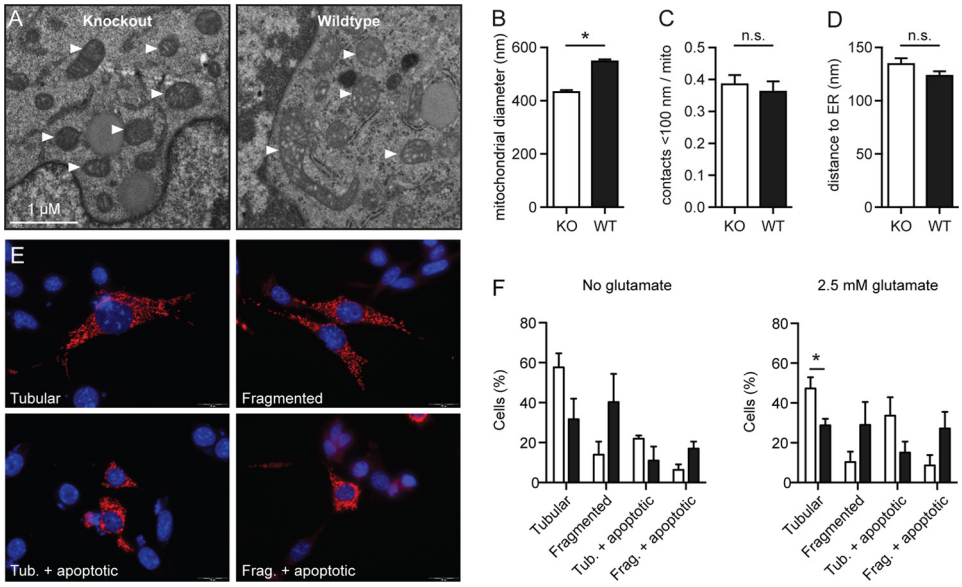

FIGURE 7. **Mitochondria of STIM1 KO cells are more densely packed and have a tubular shape.** *A*, electron microscopic images of STIM1 WT and KO MEFs were captured on a Hitachi H 600 microscope, and several morphological parameters from 523 KO mitochondria distributed over 30 visual fields and 523 WT mitochondria in 32 visual fields were quantitated and expressed as the means ± S.E. *B*, length of the mitochondrial cut surface. *C*, number of direct contacts of mitochondria to ER membranes defined by a distance of less than 100 nm divided by the number of mitochondria. *D*, distance between mitochondria and the nearest ER membrane. *E*, typical pictures of the four categories of mitochondrial shape. Healthy cells are flat and outstretched, whereas apoptotic cells appear smaller and rounded. Tubular mitochondria show a long filamentous shape, whereas fragmented mitochondria appear small and rounded. *F*, quantitative analysis of mitochondrial shape of WT and STIM1 KO cells with or without glutamate treatment (2.5 mM overnight). 100 cells of each condition were analyzed with a 60× objective and categorized by their mitochondrial shape by a blinded investigator. The *bar graphs* represent the means ± S.E. of three independently performed experiments. *n.s.*, not significant; *, $p < 0.05$, Student's *t* test. *Tub.*, tubular mitochondria; *Frag.*, fragmented mitochondria.

potential sensor TMRE. STIM1 KO MEFs exhibited significantly increased fluorescence of both Rhod2-AM (Fig. 8*A*) and TMRE (Fig. 8*B*), indicating high $[Ca^{2+}]_m$ and a higher mitochondrial membrane potential in line with the increased superoxide production shown in Fig. 5*C*. Mitochondria from STIM1 KO cells are thus elongated, densely packed, and more metabolically active, leading to an increased ROS concentration under basal conditions.

Oxidative glutamate toxicity proceeds in a well defined manner and includes release of apoptosis-inducing factor (AIF) from the mitochondria at the end of the cascade. AIF translocates to the nucleus in response to glutamate (Fig. 8*C*), where it triggers nuclear condensation and completion of the cell death program (31). Because this translocation is not only involved in endogenous oxidative stress but also dependent on the activity of the Ca^{2+}-dependent cysteine protease calpain 1 (32), we suspected that AIF might contribute to the observed susceptibility of STIM1-deficient cells to GSH depletion. In an imaging-based translocation assay, we indeed observed an increased amount of nuclear AIF relative to cytosolic AIF in STIM1 KO cells already under basal conditions, which increased in a concentration-dependent manner after glutamate treatment and always remained above WT levels in all conditions (Fig. 8*D*). Stable STIM1-EYFP expression did not serve to rescue the elevated ratio of nuclear/cytosolic AIF signal in untreated cells but impeded the translocation of AIF to the nucleus after glutamate exposure (Fig. 8*E*). Cells expressing DA-STIM1-EYFP instead showed an elevated base-line translocation of AIF together with a more pronounced translocation in response to glutamate, consistent with their increased susceptibility against oxidative stress.

DISCUSSION

Our results suggest that SOCE plays a role in cellular susceptibility to oxidative stress. We found that inhibition of SOCE by knock-out of STIM1 or knockdown of ORAI1 rendered fibroblasts more susceptible to oxidative stress, whereas re-expression of STIM1 in STIM1 KO MEFs restored SOCE activity and simultaneously protected from oxidative stress. STIM1-EYFP alone, thus without co-transfected ORAI1, did not restore SOCE to WT levels, probably because of a not-optimal ratio between STIM1 and endogenous ORAI1, which is important for SOCE (15). This is also reflected by the observation that co-transfection of ORAI1 together with STIM1-EYFP still increased the resistance of STIM1 KO cells to oxidative glutamate toxicity. We therefore conclude that the STIM1:ORAI1 ratio is difficult to adjust, which causes an incomplete repair of oxidative stress resistance. In contrast to this previous study, STIM1 was overexpressed in a STIM1-deficient background, which probably explains the effects on SOCE and cell death even in the absence of co-transfected ORAI1. It is also conceivable that the recently reported glutathionylation of STIM1 in response to oxidative stress, which results in its constitutive activation (22), renders the insufficient SOCE mediated by STIM1-EYFP rescue into just enough SOCE to be beneficial under the circumstances of glutathione depletion.

In contrast to our assumptions, we found that STIM1 KO cells contained more Ca^{2+} in the intracellular stores. In the presence of extracellular Ca^{2+}, the cytosolic Ca^{2+} concentration was reduced. This probably reflects the activity of compensating proteins like STIM2, which has been implicated in the control of cytosolic and ER Ca^{2+} levels (33), although we did

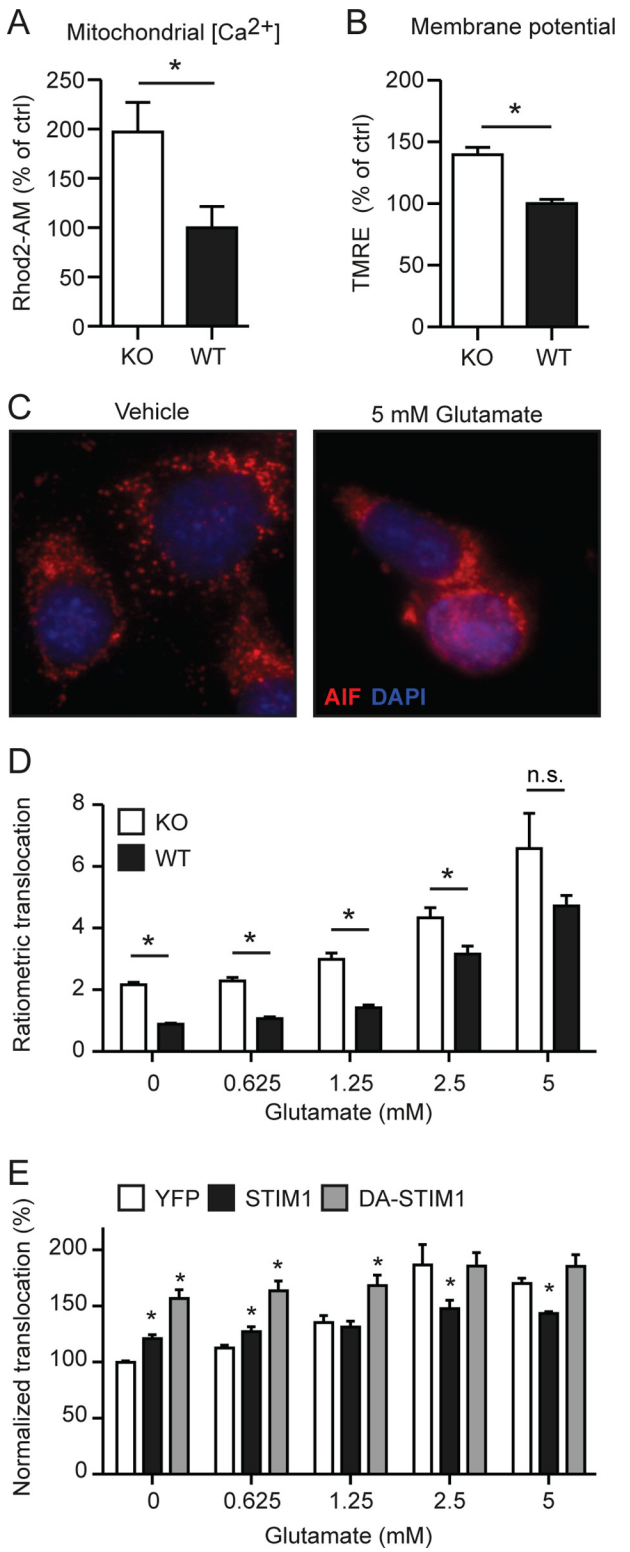

FIGURE 8. **Mitochondria from STIM1 KO cells are more metabolically active and more susceptible to nuclear translocation of apoptosis-inducing factor.** *A* and *B*, STIM1 KO MEFs show increased mitochondrial [Ca^{2+}] measured with Rhod2-AM (*A*) and increased membrane potential measured with TMRE (*B*). The mean fluorescence intensities were analyzed in triplicate on a flow cytometer in three independent experiments, normalized to WT samples, and plotted as the means ± S.E. *C*, immunocytochemistry of AIF shows nuclear translocation after 16 h of incubation with 5 mM glutamate. *D* and *E*, AIF localization was analyzed in STIM1 WT and KO MEFs (*D*) or stably empty vector (*YFP*), STIM1-EYFP (*STIM1*), or DA-STIM1-EYFP (*DA-STIM1*) transfected KO MEFs in response to glutamate (*E*). The cells were treated with indicated concentrations of glutamate for 16 h, 24 h after seeding in 96-well plates. After immunostaining, AIF fluorescence was analyzed on a BD Pathway high content imaging system, and the ratio of nuclear to cytosolic AIF signal was calculated. The *bar graphs* represent the means ± S.E. of three independent experiments each done in quintuplicate. In total, 80,099 WT and 42,750 KO cells were analyzed for *D*, and 45,238 YFP-expressing, 47,320 STIM1-EYFP expressing, and 22,092 DA-STIM1 expressing cells were analyzed for *E*. *n.s.*, not significant; *, $p < 0.05$, ANOVA with Tukey's post hoc test.

not observe any changes in the abundance of this protein (Fig. 1*B*). Alternatively, STIM1 deficiency might increase SERCA activity as a compensatory mechanism. Not all these differences were rescued by stable expression of STIM1-EYFP, probably because of the above mentioned difficulties in adjusting ORAI1 expression. DA-STIM1-EYFP, however, reversed the effects of STIM1 deficiency in regard to Ca^{2+} homeostasis; DA-STIM1-EYFP reduced the cellular Ca^{2+} content and increased the cytosolic Ca^{2+} concentration, which could be interpreted in a way that active STIM1 in the punctae inhibits SERCA activity. STIM1 and SERCA were already shown to co-localize in punctae (16) and to interact with each other upon store depletion (34). However, a physiologic inhibition of SERCA activity by STIM1 in the punctae conformation would be completely counterintuitive; active STIM1 should rather increase SERCA activity to rapidly remove cytosolic Ca^{2+} entering through SOCE. A possible explanation for such an inhibition might be that elevated amounts of reactive oxygen species, as found in DA-STIM1-EYFP-overexpressing cells, inhibit SERCA function (35) by the formation of a disulfide bond mediated via Erp57 (36), which was only recently discovered to interact with STIM1 and regulate SOCE activity (37). In any case, we think that it is very possible that such a constitutive inhibition of SERCA activity renders cells more susceptible to oxidative stress and thus mediates the detrimental effect of DA-STIM1-EYFP.

Because we observed an effect of STIM1-EYFP on oxidative stress but no significant effects on the intracellular Ca^{2+} homeostasis, we considered additional effects of STIM1 on the cellular redox regulation and analyzed the GSH content, ROS production, and expression of antioxidative defense genes in these cells. Under ideal conditions, we observed that the lack of STIM1 appeared to be even beneficial: there was an increase in cellular glutathione content, which was most likely mediated by an up-regulation of the antioxidant response through increased translocation of NRF2 to the nucleus where it binds antioxidant response elements in promoter regions and thereby triggers the expression of antioxidative defense genes. Under normal conditions NRF2 is prevented from entering the nucleus by binding to KEAP1 (24). Together with Cullin 3, KEAP1 builds an E3 ubiquitin ligase that actively targets NRF2 for degradation by the proteasome system, resulting in a very short half-life of NRF2 (38). Increased amounts of ROS as observed in STIM1 KO cells can modify reactive cysteine residues of KEAP1 releasing NRF2 and permitting its translocation to the nucleus (25). Additionally, PERK was found to be hyperphosphorylated in STIM1 KO cells, which also triggers NRF2 translocation (26) and promotes phosphorylation of eIF2α, a transcription factor enhancing expression of system Xc^- (27), an important component of the antioxidative defense machinery. In summary,

these results disclose that STIM1 KO MEFs suffer from an increased basal oxidative stress level, which promotes defense mechanisms to detoxify the high amount of ROS produced in these cells. However, under additional oxidative stress this system collapses, suggesting that this compensation is already at the edge under normal conditions or that it cannot be adapted to increased demand of antioxidant mechanisms.

Under unchallenged conditions, we also observed an increased mitochondrial Ca^{2+} concentration and a higher membrane potential. Both indicate increased mitochondrial respiratory activity probably necessary to generate ATP to run compensatory mechanisms. These changes in mitochondrial function were also accompanied by changes in mitochondrial shape and integrity. The changes in integrity mirrored the effects on protection against oxidative stress, which suggests a connection. We suspect that the increase in mitochondrial respiration, which elevates ROS production, renders the mitochondria more prone to release of AIF, which has been shown to play an imminent role in cell death mediated by glutathione depletion previously (31). We therefore conclude that the increased metabolic activity observed in STIM1 KO cells, which is probably necessary to compensate for SOCE deficiency, renders mitochondria more prone to permeabilization of the outer mitochondrial membrane and that this mediates the increased susceptibility to oxidative stress.

Our results indicate that the intact SOCE machinery enables the cell to carefully balance energy production and ROS detoxification. Loss of STIM1 or gain of function apparently precludes proper adaption to cellular energy needs and can be beneficial or detrimental depending on the cellular circumstances. This is well in line with the current literature where numerous different outcomes of cellular fate were reported in dependence of STIM1. In malignant melanoma cells or C6 glioma cells, STIM1-mediated signaling within an intact SOCE machinery was described to be essential for cell survival (20, 21). Ca^{2+}-independent activation of STIM1 through glutathionylation (22) or strong activation of SOCE on soft substrates in cervical endothelial cells (19) seems to be detrimental. These results suggest that STIM1 and SOCE play a role in the antioxidant response and are involved in the regulation of cellular energy production.

Acknowledgment—We thank Andrea Issberner for excellent technical support.

REFERENCES

1. Takemura, H., and Putney, J. W. (1989) Capacitative calcium entry in parotid acinar cells. *Biochem. J.* **258,** 409–412
2. Takemura, H., Hughes, A. R., Thastrup, O., and Putney, J. W. (1989) Activation of calcium entry by the tumor promoter thapsigargin in parotid acinar cells. Evidence that an intracellular calcium pool and not an inositol phosphate regulates calcium fluxes at the plasma membrane. *J. Biol. Chem.* **264,** 12266–12271
3. Malli, R., Frieden, M., Osibow, K., Zoratti, C., Mayer, M., Demaurex, N., and Graier, W. F. (2003) Sustained Ca^{2+} transfer across mitochondria is Essential for mitochondrial Ca^{2+} buffering, sore-operated Ca^{2+} entry, and Ca^{2+} store refilling. *J. Biol. Chem.* **278,** 44769–44779
4. Frieden, M., Arnaudeau, S., Castelbou, C., and Demaurex, N. (2005) Subplasmalemmal mitochondria modulate the activity of plasma membrane Ca^{2+}-ATPases. *J. Biol. Chem.* **280,** 43198–43208
5. Jousset, H., Frieden, M., and Demaurex, N. (2007) STIM1 knockdown reveals that store-operated Ca^{2+} channels located close to sarco/endoplasmic Ca^{2+} ATPases (SERCA) pumps silently refill the endoplasmic reticulum. *J. Biol. Chem.* **282,** 11456–11464
6. Jouaville, L. S., Pinton, P., Bastianutto, C., Rutter, G. A., and Rizzuto, R. (1999) Regulation of mitochondrial ATP synthesis by calcium. Evidence for a long-term metabolic priming. *Proc. Natl. Acad. Sci. U.S.A.* **96,** 13807–13812
7. Roos, J., DiGregorio, P. J., Yeromin, A. V., Ohlsen, K., Lioudyno, M., Zhang, S., Safrina, O., Kozak, J. A., Wagner, S. L., Cahalan, M. D., Veliçelebi, G., and Stauderman, K. A. (2005) STIM1, an essential and conserved component of store-operated Ca^{2+} channel function. *J. Cell Biol.* **169,** 435–445
8. Liou, J., Kim, M. L., Heo, W. D., Jones, J. T., Myers, J. W., Ferrell, J. E., Jr., and Meyer, T. (2005) STIM is a Ca^{2+} sensor essential for Ca^{2+}-store-depletion-triggered Ca^{2+} influx. *Curr. Biol.* **15,** 1235–1241
9. Wu, M. M., Buchanan, J., Luik, R. M., and Lewis, R. S. (2006) Ca^{2+} store depletion causes STIM1 to accumulate in ER regions closely associated with the plasma membrane. *J. Cell Biol.* **174,** 803–813
10. Zhang, S. L., Yeromin, A. V., Zhang, X. H., Yu, Y., Safrina, O., Penna, A., Roos, J., Stauderman, K. A., and Cahalan, M. D. (2006) Genome-wide RNAi screen of Ca^{2+} influx identifies genes that regulate Ca^{2+} release-activated Ca^{2+} channel activity. *Proc. Natl. Acad. Sci. U.S.A.* **103,** 9357–9362
11. Prakriya, M., Feske, S., Gwack, Y., Srikanth, S., Rao, A., and Hogan, P. G. (2006) Orai1 is an essential pore subunit of the CRAC channel. *Nature* **443,** 230–233
12. Mignen, O., Thompson, J. L., and Shuttleworth, T. J. (2008) Orai1 subunit stoichiometry of the mammalian CRAC channel pore. *J. Physiol.* **586,** 419–425
13. Zhang, S. L., Yu, Y., Roos, J., Kozak, J. A., Deerinck, T. J., Ellisman, M. H., Stauderman, K. A., and Cahalan, M. D. (2005) STIM1 is a Ca^{2+} sensor that activates CRAC channels and migrates from the Ca^{2+} store to the plasma membrane. *Nature* **437,** 902–905
14. Mercer, J. C., Dehaven, W. I., Smyth, J. T., Wedel, B., Boyles, R. R., Bird, G. S., and Putney, J. W. (2006) Large store-operated calcium selective currents due to co-expression of Orai1 or Orai2 with the intracellular calcium sensor, Stim1. *J. Biol. Chem.* **281,** 24979–24990
15. Soboloff, J., Spassova, M. A., Tang, X. D., Hewavitharana, T., Xu, W., and Gill, D. L. (2006) Orai1 and STIM reconstitute store-operated calcium channel function. *J. Biol. Chem.* **281,** 20661–20665
16. Manjarrés, I. M., Rodríguez-García, A., Alonso, M. T., and García-Sancho, J. (2010) The sarco/endoplasmic reticulum Ca^{2+} ATPase (SERCA) is the third element in capacitative calcium entry. *Cell Calcium* **47,** 412–418
17. Zhivotovsky, B., and Orrenius, S. (2011) Calcium and cell death mechanisms. A perspective from the cell death community. *Cell Calcium* **50,** 211–221
18. Sabbioni, S., Barbanti-Brodano, G., Croce, C. M., and Negrini, M. (1997) GOK. A gene at 11p15 involved in rhabdomyosarcoma and rhabdoid tumor development. *Cancer Res.* **57,** 4493–4497
19. Chiu, W.-T., Tang, M.-J., Jao, H.-C., and Shen, M.-R. (2008) Soft substrate up-regulates the interaction of STIM1 with store-operated Ca^{2+} channels that lead to normal epithelial cell apoptosis. *Mol. Biol. Cell* **19,** 2220–2230
20. Feldman, B., Fedida-Metula, S., Nita, J., Sekler, I., and Fishman, D. (2010) Coupling of mitochondria to store-operated Ca^{2+}-signaling sustains constitutive activation of protein kinase B/Akt and augments survival of malignant melanoma cells. *Cell Calcium* **47,** 525–537
21. Liu, H., Hughes, J. D., Rollins, S., Chen, B., and Perkins, E. (2011) Calcium entry via ORAI1 regulates glioblastoma cell proliferation and apoptosis. *Exp. Mol. Pathol.* **91,** 753–760
22. Hawkins, B. J., Irrinki, K. M., Mallilankaraman, K., Lien, Y.-C., Wang, Y., Bhanumathy, C. D., Subbiah, R., Ritchie, M. F., Soboloff, J., Baba, Y., Kurosaki, T., Joseph, S. K., Gill, D. L., and Madesh, M. (2010) *S*-Glutathionylation activates STIM1 and alters mitochondrial homeostasis. *J. Cell Biol.* **190,** 391–405
23. Albrecht, P., Lewerenz, J., Dittmer, S., Noack, R., Maher, P., and Methner, A. (2010) Mechanisms of oxidative glutamate toxicity. The glutamate/

cystine antiporter system Xc^- as a neuroprotective drug target. *CNS Neurol. Disord. Drug Targets* **9,** 373–382
24. Itoh, K., Wakabayashi, N., Katoh, Y., Ishii, T., Igarashi, K., Engel, J. D., and Yamamoto, M. (1999) Keap1 represses nuclear activation of antioxidant responsive elements by Nrf2 through binding to the amino-terminal Neh2 domain. *Genes Dev.* **13,** 76–86
25. Yamamoto, T., Suzuki, T., Kobayashi, A., Wakabayashi, J., Maher, J., Motohashi, H., and Yamamoto, M. (2008) Physiological significance of reactive cysteine residues of Keap1 in determining Nrf2 activity. *Mol. Cell. Biol.* **28,** 2758–2770
26. Cullinan, S. B., Zhang, D., Hannink, M., Arvisais, E., Kaufman, R. J., and Diehl, J. A. (2003) Nrf2 is a direct PERK substrate and effector of PERK-dependent cell survival. *Mol. Cell. Biol.* **23,** 7198–7209
27. Lewerenz, J., and Maher, P. (2009) Basal levels of eIF2α phosphorylation determine cellular antioxidant status by regulating ATF4 and xCT expression. *J. Biol. Chem.* **284,** 1106–1115
28. Arnaudeau, S., Kelley, W. L., Walsh, J. V., Jr., and Demaurex, N. (2001) Mitochondria recycle Ca^{2+} to the endoplasmic reticulum and prevent the depletion of neighboring endoplasmic reticulum regions. *J. Biol. Chem.* **276,** 29430–29439
29. Westermann, B. (2010) Mitochondrial fusion and fission in cell life and death. *Nat. Rev. Mol. Cell Biol.* **11,** 872–884
30. Grohm, J., Plesnila, N., and Culmsee, C. (2010) Bid mediates fission, membrane permeabilization and peri-nuclear accumulation of mitochondria as a prerequisite for oxidative neuronal cell death. *Brain Behav Immun.* **24,** 831–838
31. Landshamer, S., Hoehn, M., Barth, N., Duvezin-Caubet, S., Schwake, G., Tobaben, S., Kazhdan, I., Becattini, B., Zahler, S., Vollmar, A., Pellecchia, M., Reichert, A., Plesnila, N., Wagner, E., and Culmsee, C. (2008) Bid-induced release of AIF from mitochondria causes immediate neuronal cell death. *Cell Death Differ.* **15,** 1553–1563
32. Cao, G., Xing, J., Xiao, X., Liou, A. K., Gao, Y., Yin, X.-M., Clark, R. S., Graham, S. H., and Chen, J. (2007) Critical role of calpain I in mitochondrial release of apoptosis-inducing factor in ischemic neuronal injury. *J. Neurosci.* **27,** 9278–9293
33. Brandman, O., Liou, J., Park, W. S., and Meyer, T. (2007) STIM2 is a feedback regulator that stabilizes basal cytosolic and endoplasmic reticulum Ca^{2+} levels. *Cell* **131,** 1327–1339
34. Sampieri, A., Zepeda, A., Asanov, A., and Vaca, L. (2009) Visualizing the store-operated channel complex assembly in real time. Identification of SERCA2 as a new member. *Cell Calcium* **45,** 439–446
35. Kuster, G. M., Lancel, S., Zhang, J., Communal, C., Trucillo, M. P., Lim, C. C., Pfister, O., Weinberg, E. O., Cohen, R. A., Liao, R., Siwik, D. A., and Colucci, W. S. (2010) Redox-mediated reciprocal regulation of SERCA and Na^+-Ca^{2+} exchanger contributes to sarcoplasmic reticulum Ca^{2+} depletion in cardiac myocytes. *Free Radic. Biol. Med.* **48,** 1182–1187
36. Li, Y., and Camacho, P. (2004) Ca^{2+}-dependent redox modulation of SERCA 2b by ERp57. *J. Cell Biol.* **164,** 35–46
37. Prins, D., Groenendyk, J., Touret, N., and Michalak, M. (2011) Modulation of STIM1 and capacitative Ca^{2+} entry by the endoplasmic reticulum luminal oxidoreductase ERp57. *EMBO Rep.* **12,** 1182–1188
38. Zhang, D. D., Lo, S.-C., Cross, J. V., Templeton, D. J., and Hannink, M. (2004) Keap1 is a redox-regulated substrate adaptor protein for a Cul3-dependent ubiquitin ligase complex. *Mol. Cell. Biol.* **24,** 10941–10953